The EMBO Journal vol.15 no.20 pp.5481–5491, 1996

The 1.8 Å crystal structure of human cathepsin G in complex with Suc-Val-Pro-Phe^P-(OPh)$_2$: a Janus-faced proteinase with two opposite specificities

Peter Hof[1], Irmgard Mayr, Robert Huber, Edward Korzus[2,3], Jan Potempa[2,4], James Travis[2], James C.Powers[5] and Wolfram Bode[1]

Max-Planck-Institut für Biochemie, Am Klopferspitz 18a, D-82152 Planegg-Martinsried, Germany, [2]Department of Biochemistry, The University of Georgia, Athens, GA 30602, and [5]School of Chemistry and Biochemistry, Georgia Institute of Technology, Atlanta, GA 30332, USA

[3]Present address: Howard Hughes Medical Institute, Department and School of Medicine, University of California, San Diego, CA, USA
[4]Present address: Jagiellonian University, Institute of Molecular Biology, Al. Mickiewicza 3, 31-120 Krakow, Poland

[1]Corresponding authors

The crystal structure of human neutrophil cathepsin G, complexed with the peptidyl phosphonate inhibitor Suc-Val-Pro-Phe^P-(OPh)$_2$, has been determined to a resolution of 1.8 Å using Patterson search techniques. The cathepsin G structure shows the polypeptide fold characteristic of trypsin-like serine proteinases and is especially similar to rat mast cell proteinase II. Unique to cathepsin G, however, is the presence of Glu226 (chymotrypsinogen numbering), which is situated at the bottom of the S1 specificity pocket, dividing it into two compartments. For this reason, the benzyl side chain of the inhibitor Phe^P residue does not fully occupy the pocket but is, instead, located at its entrance. Its positively charged equatorial edge is involved in a favourable electrostatic interaction with the negatively charged carboxylate group of Glu226. Arrangement of this Glu226 carboxylate would also allow accommodation of a Lys side chain in this S1 pocket, in agreement with the recently observed cathepsin G preference for Lys and Phe at P1. The cathepsin G complex with the covalently bound phosphonate inhibitor mimics a tetrahedral substrate intermediate. A comparison of the Arg surface distributions of cathepsin G, leukocyte elastase and rat mast cell protease II shows no simple common recognition pattern for a mannose-6-phosphate receptor-independent targeting mechanism for sorting of these granular proteinases.

Keywords: crystal structure/inflammation/inhibitor/serine proteinase/specificity

Introduction

Human neutrophil elastase (hne), cathepsin G (catg) and proteinase 3 represent a major class of proteins found in the azurophilic granules of polymorphonuclear leukocytes (neutrophils), but also in monocytes (Campbell *et al.*, 1989) and in mast cells (Schechter *et al.*, 1994). These three serine proteinases are utilized by the phagocytic cells to degrade foreign organisms or dead tissues during inflammatory responses. These enzymes are unique in that they have, in addition to the ability to digest denatured proteins and polypeptides, the capacity also to degrade most constituents of the extracellular matrix (Baggiolini *et al.*, 1979; Caughey, 1994; Gabay, 1994). Indeed, it has recently been shown that both hne and catg activities can also be located on the surface of neutrophils, suggesting alternative functions for these proteinases in cellular processes such as egress from the vasculature and penetration of tissue barriers during chemotactic responses (Owen and Campbell, 1995).

During the process of phagocytosis there is substantial release of these three proteinases from azurophilic granules, both intracellularly into vacuoles containing materials to be degraded, and extracellularly as a result of cell leakage and/or neutrophil death. Usually, there are significant levels of plasma-derived proteinase inhibitors such as α1-proteinase inhibitor and α1-antichymotrypsin to inhibit extracellular proteinases. However, at inflammatory sites, genetic or acquired deficiencies of host tissue inhibitors can result in the uncontrolled digestion of healthy tissues and, ultimately, in the development of connective tissue diseases, such as emphysema and periodontitis. Hereditary deficiency of α1-antichymotrypsin, the major physiological inhibitor of catg (Beatty *et al.*, 1980), has been shown to be a risk factor for lung disease (Faber *et al.*, 1993). It has been suggested that the rapid and dramatic increase in α1-antichymotrypsin, after inflammatory episodes and the subsequent extracellular release of catg, is needed to control its rapid angiotensin I-converting activity (Reilly *et al.*, 1982; Snyder *et al.*, 1985; Travis, 1988; Bangalore and Travis, 1994).

The physical and chemical properties of catg are now well understood. According to its sequence and occurrence, human catg is a typical member of the haematopoietic serine proteinase superfamily, with particularly close sequence relationships to human granzyme H (Haddad *et al.*, 1991), granzyme B (also known under other designations such as Cytotoxic Cell Protease 1; see for example Jenne *et al.*, 1989; Chandrasekharan *et al.*, 1996) and rat mast cell protease II (rmcp; Salvesen *et al.*, 1987). Human catg is synthesized as a 255 amino acid residue protein including an 18-residue signal peptide and a two-residue activation peptide at the N-terminus (Salvesen *et al.*, 1987). Removal of the Gly Glu propeptide upon proteolytic activation of catg, probably brought about by the thiol proteinase dipeptidyl peptidase I (McGuire *et al.*, 1993), gives rise to the characteristic Ile16 N-terminus of the mature enzyme. Further slow proteolytic processing of the C-terminal peptide extension of catg, presumably occurring at Ser244-Phe245 or shortly behind, has been reported (Salvesen and Enghild, 1990; Gullberg *et al.*, 1994). Human catg can be isolated in multiple isoforms,

which seem to differ mainly in type and content of the sugar linked to its single N-glycosylation site.

Catg has been found to hydrolyse synthetic substrates much more slowly than comparable proteinases such as hne. Catg was thought to possess a strict chymotrypsin-like specificity, with a substantial preference for peptide substrate cleavage C-terminal of P1-Phe (Powers *et al.*, 1985; Tanaka *et al.*, 1985). It was recognized only after the crystal structure determination of hne (Bode *et al.*, 1986) that the presence of an acidic residue in the S1 pocket might result in the hydrolysis of substrates with basic P1 residues. Indeed, more recent kinetic studies verified that Phe can be substituted by Lys, giving rise to similar k_{cat}/K_m values (Powers *et al.*, 1989). Physiologically, the proteolytic activity of catg seems to be mainly controlled by the serpin α1-antichymotrypsin (Beatty *et al.*, 1980), but also the endogenous inhibitors α1-proteinase inhibitor and mucus proteinase inhibitor form stable complexes with catg (Schiessler *et al.*, 1976). It has been shown that catg and low-molecular weight heparin form a 1:1 complex, which is inhibited only extremely slowly by α1-antichymotrypsin and α1-proteinase inhibitor and which resists inhibition by eglin c (Ermolieff *et al.*, 1994). *In vitro*, catg has also been inactivated by a number of different classes of synthetic serine proteinase inhibitors (for reference, see Powers and Harper, 1986). A particularly useful class of inhibitors in X-ray crystallography are α-aminoalkylphosphonate diphenyl esters since they are stable for many days under most conditions (Oleksyszyn and Powers, 1994). These transition-state analogue inhibitors irreversibly inhibit serine proteinases by phosphonylation of the active-site serine to form a phosphonated Ser195 derivative which again is stable for days.

Although catg is apparently less active endoproteolytically than hne or proteinase 3, it can degrade connective tissue components such as cartilage proteoglycans, collagen type I and II, laminin and fibronectin. Catg also has other unusual physiological characteristics, however. In particular, it has significant broad-spectrum antimicrobial activity, which is independent of its function as a proteinase. A catg digestion peptide mixture, obtained by clostripain treatment, retained part of that bactericidal activity (Bangalore *et al.*, 1990). In addition, the enzyme has been suggested to be involved in IL-8 processing (Padrines *et al.*, 1994), in generation of amyloidogenic fragments from the β-amyloid precursor protein (Savage *et al.*, 1994), in strong interactions with the V3 loop of HIV-1 gp120 (Avril *et al.*, 1994, 1995), in proteolytic activation of complement C3 (Maison *et al.*, 1991), in cellular effects on platelets via degradation and/or activation of a thrombin receptor or another homologous receptor (Selak, 1994; Molino *et al.*, 1995), in activation of human factor V (Allen and Tracy, 1995) and in stimulation of human lymphocytes (Hase-Yamazaki and Aoki, 1995). In most of these examples catg seems to cleave after Phe residues.

In an attempt to understand the physiological and chemical properties of catg at atomic resolution, we have solved its crystal structure in complex with the phosphonate inhibitor Suc-Val-Pro-Phe^P-$(OPh)_2$. Here, we give a detailed description of the structure, emphasizing especially its peculiar specificity and relevance to possible structure-based drug design. Furthermore, this structure will be an excellent template for modelling structures of the homologous granzymes.

Results

Overall structure

Catg resembles an oblate ellipsoid with diameters of ~35 and ~50 Å. It is folded into two six-stranded β-barrels strapped together by three *trans* domain segments. The surface is made up of various turn structures, two short α-helical single turns from residues 56 to 58 and 165 to 168, and the C-terminal helix from residue 231 to 243 (see Figure 1). As in the other trypsin-like serine proteinases (Bode and Huber, 1986), the active-site cleft and the catalytic residues are located along the junction of both barrels.

Optimal superposition of the catg structure with rmcp (Remington *et al.*, 1988), hne (Bode *et al.*, 1986), bovine chymotrypsin (chymo; Blevins and Tulinsky, 1985) and bovine β-trypsin (trypsin; Bode and Schwager, 1975) results in 204, 173, 178 and 182 topologically equivalent α-carbon atoms with r.m.s. deviations of 0.55, 0.66, 0.77 and 0.67 Å, respectively, if only α-carbon atom pairs within 1.5 Å are included. These data show the ranking with respect to topological homology to catg: rmcp is most similar, followed by trypsin and hne. This order is strengthened if identical residues are compared: 109 topologically equivalent catg residues are identical with rmcp, compared with 77, 73 and 75, respectively, for the three other proteinases. The topological equivalence forms the basis for the alignment of the five serine proteinases shown in Table I; the numbering of catg is based on the equivalence with chymotrypsinogen (Hartley and Shotton, 1971). A proper alignment with chymo requires single-residue insertions at positions 184A, 187A and 220A, and deletions of one, two, three and four residues at chymo positions 62, 149–150, 221–223 and 203–206, respectively. Compared with rmcp, only one single-residue deletion and one single-residue insertion have to be applied. The optimal superposition with hne, in contrast, requires several longer deletions and insertions (see Table I).

Like all active chymotrypsin-like serine proteinases, the catg sequence starts with Ile16, with its ammonium group forming an internal salt bridge with the side chain carboxylate group of Asp194. A pentapeptide comprising the first five N-terminal residues of catg (Ile-Ile-Gly-Gly-Arg) was found to possess antimicrobial activity (Bangalore *et al.*, 1990). In the intact catg molecule these first two residues are buried and the peptide chain is accessible to the solvent only from Gly18 onwards. The last residue of the catg polypeptide chain, which is (partially) defined in the electron density, is Ser244. Although this is consistent with possible disorder of the C-terminal peptide extension, the crystal packing does not appear to allow space for the additional 11 residues. We therefore assume that the crystallized catg is C-terminally truncated, ending either at Ser244 (in agreement with Salvesen and Enghild, 1990) or at Phe245 (which represents an autocatalytic cleavage site).

With its 34 arginine and four lysine residues opposed by only 11 glutamates and nine aspartates, catg is an extremely basic molecule. Apart from Asp102, Asp194

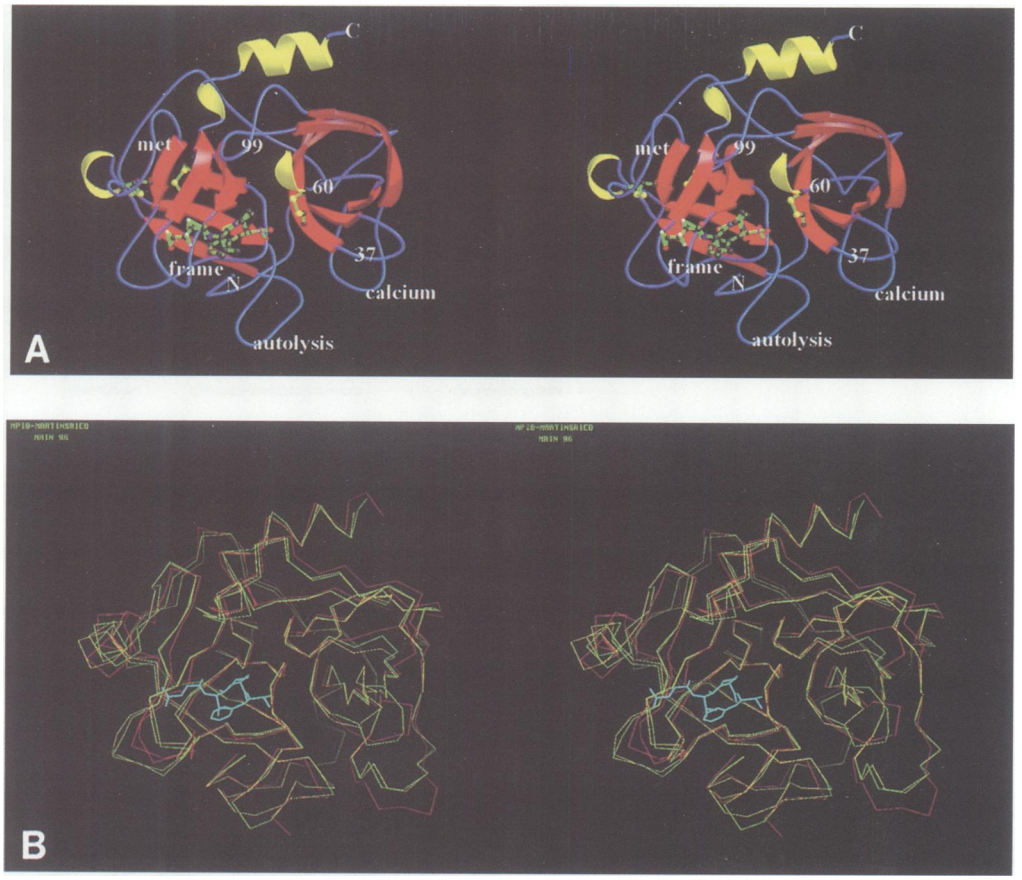

Fig. 1. (**A**) Stereo ribbon plot of human cathepsin G. The view (referred to as standard orientation) is towards the active-site cleft, which runs from left to right across the molecular surface. The Suc-Val-Pro-Pho^{P} inhibitor and the disulfide bridges are depicted as ball-and-stick models. Figure made with MOLSCRIPT (Kraulis, 1991) and rendered with RASTER3D (Merritt and Murphy, 1994). (**B**) Superposition of the Cα stereo plots of chymo (red), rmcp (yellow) and catg (green). The view is the standard view as in (A). The phosphonate inhibitor has been added (blue) as bound to catg. The figure was prepared employing MAIN (Turk, 1992).

and Glu226, involved in the catalytic triad, in internal salt bridge formation, and buried in the S1 pocket (see below), respectively, all charged side chains are at least partially exposed to the bulk solvent. The juxtaposition of Glu226, Asp102 and Asp194 produces together a rather negative electrostatic potential in the specificity pocket (see Figure 2). In the immediate vicinity of the active site, three arginine residues reside (Arg97 to the north, and Arg41 and Arg143 to the south), while in its more distant neighbourhood Arg178, Arg179 and Arg187A (to the west) and Arg147, Arg148 (to the south) can be located (see Figure 2). Only two of the Arg side chains (Arg27 and Arg48) are involved in surface-located, intramolecular salt bridges with carboxylate groups (Glu157 and Asp50). None of the other guanidino groups is compensated by neighbouring counter charges of the protein. Most of the arginines are arranged in a U-shape around the front side of the molecule (as shown in Figure 2) and on the surface site opposite to the active-site cleft (figure not shown). Several of these arginines are clustered in surface patches consisting of two to six closely packed guanidino groups (such as Arg164, 166, 170, 185 and 186 arranged around the intermediate helix located to the west in Figure 2, and Arg110, 111, 48, 113, 114 and 116 positioned on the backside of the molecule).

Loops surrounding the active site

Since many of the distinct properties of serine proteinases arise from the loops making up the active site, these deserve particular attention; in the following they will be addressed in an anticlockwise manner using the 'front' view of catg given in Figure 1 as a standard orientation.

To the east of the active site (quarters denoted according to the standard orientation) the 37 insertion loop apparently projects out of the molecular surface near the active-site cleft (see Figure 2); no electron density is observed, however, for five residues from 36 to 38 (they are nevertheless included in Figures 1 and 2 to preserve chain continuity). Segment 39–41 narrows the active-site cleft much more than observed in most other serine proteinases, but is similar to the equivalent segment of rmcp. Residue 32 is Tyr and residue 40 is Ser; thus, catg lacks a specific 'zymogen triad', Asp194-His40-Ser32, as present in trypsin or chymo, to stabilize the zymogen form. From residue 41 on, all the proteinases compared here take the same path; only in rmcp and catg do the side chains of residue 41 project towards the active site, however. From Cγ on, the side chain of Arg41 in catg is flexible, allowing some adaptation to bound 'primed' substrate residues. This backbone path alters the primed subsites in catg compared with most other trypsin-like serine proteinases;

Table I. Sequence alignments

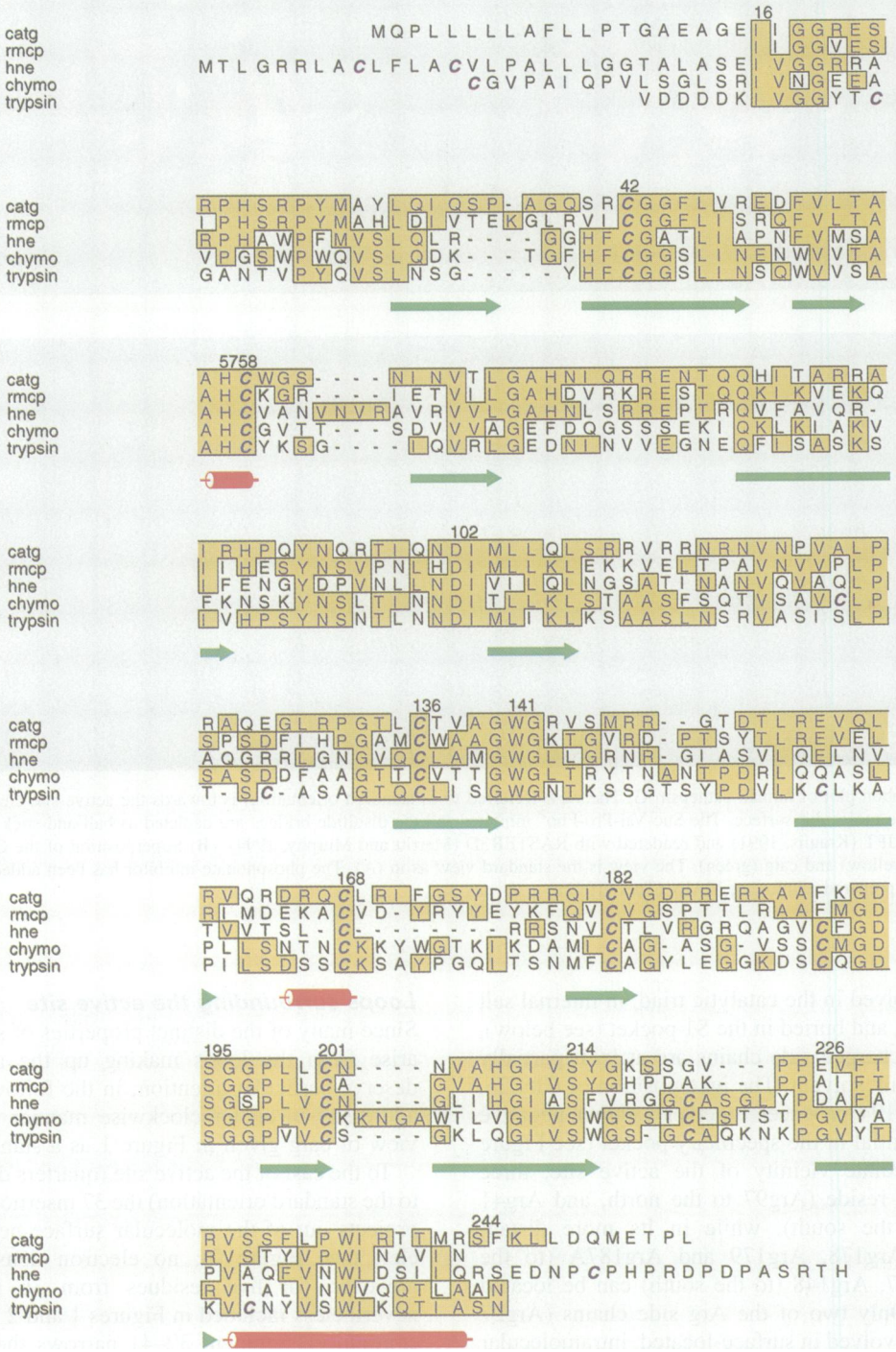

Human cathepsin G (catg; Salvesen *et al.*, 1987), rat mast cell protease II (rmcp; Woodbury *et al.*, 1978), human leukocyte elastase (hne; Sinha *et al.*, 1987), bovine chymotrypsinogen (chymo; Hartley and Shotton, 1971) and bovine β trypsin (trypsin; Mikes *et al.*, 1966), made according to their topological equivalence. The numbers refer to chymotrypsinogen. The table was prepared with ALSCRIPT (Barton, 1993).

the third domain of turkey ovomucoid inhibitor bound to catg in its binding configuration with hne would clash with this catg segment.

North of and adjacent to the 37 loop resides the 60 loop, which extends along the molecular body in similar manner to that observed in rmcp and trypsin. The indole moiety of Trp59 extends toward the bulk water, but makes plane-to-plane stacking interactions with the guanidino group of the adjacent Arg90. The side chain of Asn65, which represents the single carbohydrate linkage site of catg, is distant from the active-site cleft, and points away from it. An oligosaccharide should therefore not interfere with productively bound macromolecular substrates, in agreement with the negligible effects of glycosylation on

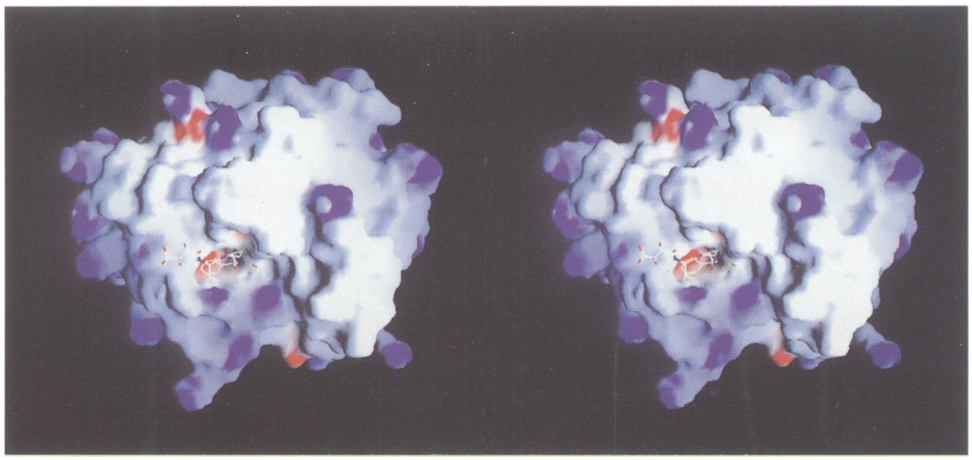

Fig. 2. Solid surface stereo representation of the electrostatic potential of the 'front' side of catg shown in standard orientation. Colouring is made according to the calculated electrostatic potential contoured from –20 kT/e (intense red) to 20 kT/e (intense blue). The inhibitor is depicted as a stick model. Visible is the clustering of positive charges (mainly originating from Arg residues) to the south of the active site and in a U-shape around the 'front' side. Figure made with GRASP (Nicholls *et al.*, 1993).

catg activity. Some broken electron density might indicate glycosylation at Asn65; however, because this density lacks any characteristic sugar-like shape, it has been interpreted by water molecules.

As in other serine proteinases, the β-hairpin loop of catg (His91–Ile99) protrudes from the north rim into the active site (Figure 2). Its N-terminal part (His91–Arg97) contains a peptide segment for which antimicrobial activity has been shown. Further to the west, the Cys168–Cys182 loop is linked to the 99 loop through the most exposed Ser174. Contrary to its general designation as a 'methionine' loop, the usual position for Met, 180, is occupied in catg by a Gln.

South of this loop is segment 217–225, which appears from the molecular structure from Lys217 to Gly220 to be similar to rmcp and chymo. Like most other granula-associated chymases, including rmcp, catg lacks cysteine residues at positions 191 and 220, which in most other chymotrypsin-like serine proteinases form a disulfide bridge. Instead, catg has characteristic Gly220 and Phe191, with the phenyl ring of the latter approximately occupying the site of the disulfide bridge. The conformation and position of segment 189–192 remain largely unaffected by this important structural difference. The following segment Val221–Pro224–Pro225 is two residues shorter compared with chymo. Similar to rmcp, the peptide group between Pro224 and Pro225 is in a *cis* conformation; the other three proteinases compared have a longer loop, lack a proline at position 224 and possess a *trans*-proline at position 225.

The southern boundary of the active-site cleft of catg is mainly formed by the fully defined 'autolysis' loop. This loop, which in catg is two residues shorter than in chymo and seems to be resistant to cleavage, packs against the molecular body by looping around the side chain of Arg143. Adjacent to this 'autolysis' loop and behind the 37 loop resides the 70–80 loop. In catg this loop is topologically similar to the calcium-binding loops of trypsin and of related proteinases (Bode and Schwager, 1975). In contrast to the digestive enzymes and the clotting factors IXa (Brandstetter *et al.*, 1995) and Xa (Padmanabhan *et al.*, 1993), however, the calcium site is occupied in catg by the carboxamide nitrogen of Gln80, which is in hydrogen bond distance to the carbonyl oxygen of Asn72 and to one of the carboxylate oxygen atoms of Glu77. This is reminiscent of the equivalent loops in rmcp (Remington *et al.*, 1988) and hne (Bode *et al.*, 1986), where likewise position 80 is occupied by a Gln and an Arg residue, respectively, with the distal polar groups replacing the calcium ion. Replacement of the calcium by protein side-chain groups confers on these enzymes a stability which is independent of the calcium level.

Active-site cleft

The active-site cleft is bordered on the north by four exposed loops, namely a bulge in the 174 loop, the protruding loop segment 94–99, the N-terminal part of the 60 loop and segment 39–41 of the 37 loop (Figure 3). The south edge of the cleft is formed by the bulged loop 217–220, the extended side chain of Lys192, the side chains of the flat 'autolysis' loop and the 'calcium-binding' loop.

The residues of the active-site triad, Ser195, His57, Asp102 and other catalytic structures such as the oxyanion hole are arranged at the centre of the cleft exactly as in trypsin and chymo. The specificity pocket (S1) to the west of Ser195 is bordered by segments Val213–Gly220 (the entrance frame), Gly189–Ser195 (the basement), Pro225–Tyr228 (the back of the pocket) and the Phe191 side chain (closing the pocket towards the south) (see Figure 3). At its bottom this S1 pocket is subdivided by the side chain of Glu226 into two separate subcompartments. The carboxylate group of this Glu226 is fixed via two hydrogen bonds to the carbonyl oxygen and the amide nitrogen of Ala190 (2.7 and 2.9 Å, respectively). In this catg structure this geometry suggests protonation of this carboxylate group, which therefore might have a pK value shifted to considerably higher values.

To the north of this pocket, a shallow hydrophobic surface depression extends along the side chains of Phe172 and Tyr215, demarcated to the north by the amide nitrogens of residues 173 and 174 and the carbonyl groups of residues 97 and 98. The eastern side of this depression (S4 subsite) is constricted and bordered by the side chains

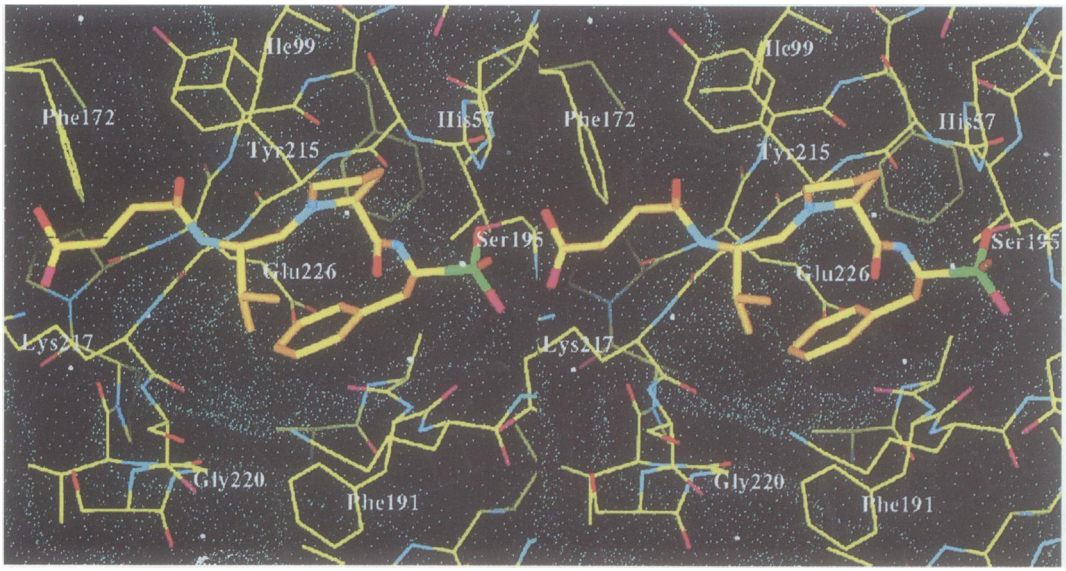

Fig. 3. Stereo stick model of the catg–inhibitor complex around the active-site cleft. The colours used are yellow for the carbon atoms of the protein, orange for those of the inhibitor, red for oxygen atoms, blue for nitrogen atoms and green for the phosphorus. A Connolly dot surface around the protein part is represented by blue dots. Water molecules are drawn as white balls. The phosphorus atom is covalently bound to the Oγ of Ser195. To the west of Ser195 opens the specificity pocket, which is divided at its bottom into two subcompartments by the side chain of Glu226. Its carboxylate group is in edge-to-edge contact with the benzyl side chain of PhoI4. The figure was prepared employing MAIN (Turk, 1992).

of Ile99 and the plane of the His57 imidazole ring forming the S2 pocket.

In contrast to most other serine proteinases, where the side chain of residue 41 (often Phe) is buried in the interior of the molecule, the Arg41 side chain of catg is exposed toward the active-site cleft. Together with the presence of the similarly exposed Ser40, a narrow crevice (S1′) is formed east of Ser195. The S3′ subsite is flattened because of the peculiar backbone path 39–41 of catg mentioned above.

Inhibitor binding

Figure 4 presents our residue notation for the α-amino-alkylphosphonate diphenyl ester inhibitor Suc-Val-Pro-Phe^{P}-(OPh)$_2$ covalently bound to catg. The continuous electron density between the phosphorus atom and Ser195 Oγ and the distance of 1.6 Å between both atoms unequivocally indicate formation of a covalent bond. There is absolutely no density accounting for the phenyl rings of the two phenoxy groups; thus, both phenyl groups seem to be lost in the catg–inhibitor complex during or after the reaction with Ser195; both phosphonate oxygens and the Ser195 Oγ are well defined by electron density (see Figure 5), however. The clear electron density indicates unambiguously a tetrahedral geometry of the phosphorus atom. One of the phosphonate oxygens is inserted into the oxyanion hole and forms hydrogen bonds to the amide nitrogen atoms of Gly193 and Ser195, while the second one is directed towards the bulk water.

The inhibitor backbone juxtaposes catg segment Ser214–Lys217 in an antiparallel, slightly twisted manner; ValI2 N and O form favourable hydrogen bonds with Gly216 O and N (3.3 Å and 2.8 Å), and a third hydrogen bond is formed between the PhoI4 amide nitrogen and the carbonyl oxygen of Ser214 (3.0 Å). As clearly shown by the electron density (Figure 5), only the L stereoisomer of the Pho residue is bound to catg. Its benzyl side chain is sandwiched between the peptide groups of Tyr215–

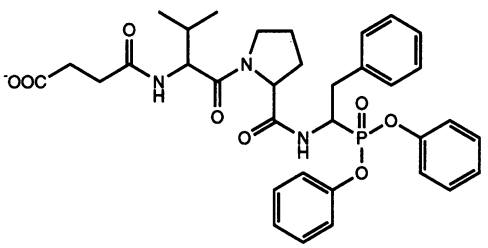

SucI1 ValI2 ProI3 PhoI4(OPh$_2$)

Fig. 4. Chemical structure of the inhibitor Suc-Val-Pro-Phe^{P}-(OPh)$_2$.

Gly216 and Ala190–Lys192; due to the partial fill of the bottom of the S1 pocket by Glu226, however, the benzyl moiety does not project towards the back of this pocket, but stays in its outer compartment, so that it is not fully sandwiched by the pocket (see Figure 3). The phenyl ring is in edge-to-edge contact with the carboxylate group of Glu226, thus allowing favourable electrostatic interactions between the positive part of the multipole field of the aromate and the partial negative charge of the carboxylic acid group. The back of either subcompartment is occupied by a fixed buried solvent molecule.

The P2 residue ProI3 of the inhibitor is kinked, which allows an optimal adaptation to the course of the active-site cleft of catg. The pentameric pyrrolidine ring of ProI3 nestles into the S2 pocket of catg and fills it completely. The isopropyl side chain of the P3 residue ValI2 extends away from the molecular surface, with its side chain atoms in weak van der Waals contacts with the catg side chains of Ser218 and Lys192. It is interesting to note that the distal ammonium group of this surface-located Lys192 does not hydrogen bond to the carbonyl group of ProI3. The Nα substituted succinyl group (SucI1) is extended along catg segment 216–217, interacting via van der Waals contacts with its bound catg molecule; its distal carboxylate

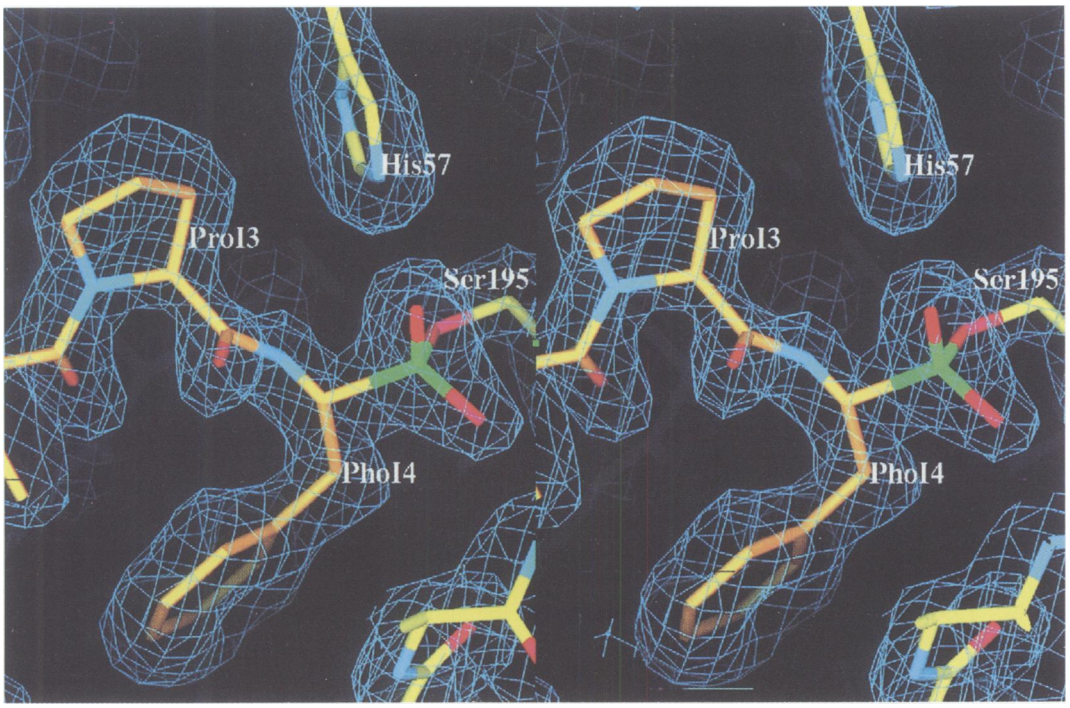

Fig. 5. Stereo section of the model around the PhoI4 residue including the final $2F_{obs}$–F_{calc} electron density contoured at 1 σ. The atom colours are the same as in Figure 3. The phosphorus atom of the inhibitor exhibits a tetrahedral geometry. Figure made with MAIN (Turk, 1992).

group forms a central 2O–2N salt bridge with the guanidyl group of Arg178 of a symmetry-related molecule. This intermolecular salt bridge might be important for crystal contacts and could be the reason for the successful crystallization of this catg–inhibitor complex.

Discussion

With the catg described in this paper the crystal structure of a third member of the granula-associated proteinases has been elucidated, after those of hne (Bode *et al.*, 1986; Wei *et al.*, 1988; Navia *et al.*, 1989; Bode, 1996) and rmcp (Remington *et al.*, 1988). In agreement with the larger sequence homology, the overall topology of catg turns out to be most similar to rmcp, so that an optimal sequence alignment, based on topological equivalence, requires only one single-residue insertion and one single-residue deletion (see Table I). However, catg also resembles rmcp most with respect to some characteristic structural details, such as the lack of a disulfide bridge between residues 191 and 220, the bulged segment 217–220 which shields the S1 pocket against the bulk water or segment 39–41 which specifically shapes the primed subsites. Consistent with its lower sequence similarity, the hne structure deviates from catg to an extent similar to trypsin and chymo. These topological similarities are in good agreement with the evolutionary relationships, reflected by the different locations of the genes coding for these proteinases on either chromosome 14 (catg and rmcp) or chromosome 19 (hne and proteinase 3).

Maximum parsimony analyses of haematopoietic proteinases revealed that human catg clusters particularly with human granzyme H, human and mouse granzyme B, and mouse granzyme C (see for example, Haddad *et al.*, 1991; Chandrasekharan *et al.*, 1996). Due to its unique cleavage specificity for peptide bonds C-terminal of acidic side chains, granzyme B involved in cytotoxic T lymphocyte-mediated lysis of target cells has attracted particular attention. Comparative model building based on the structures of chymo and trypsin, *Streptomyces griseus* trypsin and rmcp led to a model which allowed the explanation of its substrate specificity by the presence of an Arg residue at position 226 (Murphy *et al.*, 1988; Caputo *et al.*, 1994). Our catg structure would provide an even better template for modelling granzyme B; such a model would not give the detailed conformation of the side chain of Arg226 in the S1 pocket, however, for which an experimental structure would be required.

Indeed, shape and equipment of the S1 pocket of catg and its interaction with the P1-Pho residue of the bound phosphonate inhibitor are the most valuable results obtained from this catg structure analysis. This pocket is unique in that the Glu226 side chain extends into it and subdivides its bottom part into two separate subcompartments. Due to a considerable movement of the main chain away from the pocket, the distal carboxylate group of Glu226 almost exactly superimposes with the equivalent group of the shorter Asp226 side chain of hne. In contrast to hne, where the carboxylate group is fully shielded by the bulky hydrophobic side chains of Val216 and Val190 (Bode *et al.*, 1986; Bode, 1996), the Glu226 side chain of catg is exposed in the S1 pocket. Its carboxylate group is not directed towards an inserting side chain, however, but towards Ala190 of the opposite strand and fixed to it through two hydrogen bonds.

Due to this geometry of the bottom part of the catg pocket, the phenyl group of PhoI4 cannot insert to the same extent as the phenyl group of the benzamidine inhibitor does in trypsin (Bode and Schwanger, 1975); therefore it does not seem to be sandwiched optimally by the catg peptide segments forming the ceiling and the floor of this pocket. The subsite mapping experiments

show, however, that Phe residues at P1 render peptides into good catg substrates, i.e. must help to fix them in an appropriate position with respect to the catalytic residues for effective cleavage. We explain this beneficial property of Phe by the favourable electrostatic interactions between the positively charged equatorial plane edge of the phenyl group and the carboxylic acid group of Glu226.

According to Tanaka *et al.* (1985), catg cleaves synthetic peptides also behind Leu, Met and Trp, with much-reduced k_{cat}/K_m values than observed for Phe, however. The medium-sized hydrophobic side chains of Leu and Met could be accommodated in the open part of the catg pocket by using the hne-like 'back' subcompartment, under unfavourable burying of polar/charged groups at the bottom of the pocket. This capability of catg to accommodate Leu and Met side chains would be in agreement with the (tight and fast) interactions with α1-antichymotrypsin and α1-proteinase inhibitor, respectively, and with the low but significant catg affinity for a BPTI variant with Leu at P1 and Phe or Tyr at P2′ (Brinkmann *et al.*, 1991). The indole moiety of a Trp-P1 residue would not have enough room to be sandwiched into the S1 pocket in the same geometry as observed for the PhoI4 side chain. This structure thus explains the poor ability of catg compared with chymo to cleave behind Trp residues.

The presence of Glu226 at the bottom of the pocket, on the other hand, gives good structural ground for the newly found ability of catg to cleave effectively after Lys residues. A surprise, in particular when considering the reasonable affinity of the BPTI-variant with Leu at P1 and Phe or Tyr at P2′ mentioned above, is the very low association constant of native BPTI (Fioretti *et al.*, 1993) with Lys at P1. Preliminary model building studies show that a Lys P1 side chain could insert into the catg S1 pocket such that its distal ammonium group would be placed beside (anti-oriented to) the exposed oxygen of the Glu226 carboxylate group towards the 'front' subcompartment, thus allowing undisturbed hydrogen bond and salt bridge formation. In agreement with experimental results, such modelling would also suggest the favourable fit of the longer thiohomolysine side chain (Powers *et al.*, 1989). In hne, in contrast, the equivalent carboxylate of Asp226 is not accessible to elongated basic side chains (Bode, 1996), making the virtual inactivity of hne towards substrates with a Lys residue at P1 conceivable (Powers *et al.*, 1989).

The structure of the catg complex shows that the L-Pho stereoisomer of the Suc-Val-Pro-Phe^P-$(OPh)_2$ inhibitor has been selected from the D,L-racemate upon binding. The inhibitor is unequivocally covalently linked with the tetrahedral phosphonate, and thus this irreversible inhibitor is mimicking the tetrahedral transition state formed during the acylation and deacylation of peptide substrates by catg. The His57 is properly oriented to donate a proton to the leaving group. During the inhibition reaction, both phenoxy groups have been lost, the first by phosphonylation of Ser195 and the second by an ageing process. A similar result has been observed in the case of a trypsin–phosphonate complex (Bertrand *et al.*, 1996). It is likely that the His57 participates in this ageing reaction by protonation of the second phenoxy group in a manner similar to that observed during peptide bond hydrolysis.

Catg is characterized by an extremely large number of positively charged residues, mostly arginines. These Arg residues are not uniformly distributed over the catg surface, but are clustered in several positively charged surface patches, mostly distant from the active site. These exposed Arg residues are possible anchoring sites for fixing catg to the heparin and chondroitin sulfate proteoglycans which coat the inner wall of the azurophilic storage granules. Within the granules this fixation of Arg residues located near the active site could further inactivate catg, augmenting inactivation from the low granule pH. A similar electrostatic interaction with these Arg residues would also explain the reduction of the enzymatic activity of catg upon heparin binding and the enormously slow inhibition rate of such catg–heparin complexes towards α1-antichymotrypsin (Ermolieff *et al.*, 1994). The weaker heparin effects found for hne (Frommherz *et al.*, 1991) would be in agreement with the lack of Arg residues around the active site of hne (Bode, 1996). It is less easy, however, to explain the formation of 1:1 complexes with heparin for both enzymes on the basis of these crystal structures.

The mechanisms of trafficking of catg and related enzymes to their target granules remain unresolved. Recently it has been shown that granular sorting of catg occurs also in transfected cells which produce catg mutants lacking the oligosaccharide chain (Garwicz *et al.*, 1995). Thus, the mannose-6-phosphate receptor-dependent targeting postulated for granzymes A and B (Griffiths and Isaaz, 1993), is apparently not used for catg. The distinct Arg distribution of catg could represent one recognition pattern for such a mannose-6-phosphate receptor-independent targeting mechanism. A visual comparison of the Arg distribution of catg with that of hne and rmcp (which should be sorted according to similar mechanisms) shows, however, no simple common pattern which could serve for this purpose.

The catg structure shows furthermore that both constituent catg peptides, for which antibacterial activity had been shown (Bangalore *et al.*, 1990), are to a large extent located on the surface of the catg molecule and have well-defined structures. The first two residues of the pentapeptide (Ile16-Ile-Gly-Gly-Arg), derived from the N-terminus of catg, differ from the equivalent hne segment, which lacks such activity, only by the second (Ile or Val) residue. In intact catg the side chain of this Ile is only marginally exposed to the surface, so that a differentiating contact with bacteria without structural rearrangement is difficult to understand. The second catg peptide (His91-Pro-Gln-Tyr-Asn-Gln-Arg), to which bactericidal activity had been assigned, is derived from a polypeptide segment which extends into the 99 loop. In catg it is positioned to the north of the active-site cleft and very exposed to the solvent, but is very similar to that observed in the other non-bactericidal chymotrypsin-like proteinases. Thus, the antibacterial activity of this peptide must be specific to its distinct amino acid sequence. Systematic amino acid substitutions in this peptide showed that the initial His residue might be of particular importance for this activity, in agreement with the bactericidal activity found for a similar heptapeptide derived from granzyme B (Shafer *et al.*, 1991).

In conclusion, the tertiary structure of catg demonstrates

Table II. Statistics for data collection and refinement

Spacegroup	$P2_12_12_1$
Cell constants (Å)	
a	40.04
b	63.61
c	79.72
Limiting resolution (Å)	1.80
Reflections measured	68 129
R_{merge} (%)[a], overall	5.7
R_{merge}(%)[a], outermost (1.86–1.80 Å) shell	32.7
Unique reflections	18 433
Completeness (%), overall	95.1
Completeness (%), outermost (1.86–1.80 Å) shell	95.3
Non-hydrogen protein atoms	1786
Non-hydrogen inhibitor atoms	34
Solvent molecules	145
Reflections used for refinement	17 840
Resolution range (Å)	6.0–1.8
Completeness (%),overall (6.0–1.80 Å)	94.2
Completeness (%), outermost (1.82–1.80 Å) shell	92.7
R-value (%)[b], overall (6.0–1.80 Å)	19.0
R-value (%)[b], outermost (1.82–1.80 Å) shell	32.67
R-value (%)[b] without 10% data of R_{free}	18.5
Outermost (1.86–1.80 Å) shell (%)	32.27
R_{free} (%)[c]	24.02
Outermost (1.86–1.80 Å) shell (%)	34.75
R.m.s. standard deviations	
bond length (Å)	0.013
bond angles (°)	1.765
average B-value/SD[d] (Å^2)	22.43/2.05

[a] $R_{merge} = [\Sigma_h \Sigma_i |I(h.i) - <I(h)>| / \Sigma_h \Sigma_i I(h.i)] \times 100$ where $I(h.i)$ is the intensity value of the *i*th measurement of *h* and $<I(h)>$ is the corresponding mean value of *h* for all *i* measurements of *h*: the summation is over all measurements.
[b] $R_{cryst} = (\Sigma|F_o - F_c|/\Sigma F_o) \times 100$.
[c] R_{free} was calculated randomly omitting 10% of the observed reflections from refinement and R-factor calculation (see text).
[d] Standard deviation is from bonded atoms.

that the enzyme exhibits a unique Janus-like double-headed substrate specificity. Utilizing this structural knowledge, it should be possible to design novel inhibitors which would make use of the unique S1 specificity pocket. Additional inhibitor interactions could be obtained by designing inhibitors which would extend into S1′ subsites.

Materials and methods

Cat G was purified from extracts of granules of human polymorphonuclear leukocytes according to methods previously described (Baugh and Travis, 1976; Travis *et al.*, 1978). A mixture of isoforms differing only in carbohydrate content was further resolved by FPLC into individual components, which were complexed with various inhibitors and utilized for crystal growth. Only a mixture of catg isoforms complexed with a racemic mixture of L,D-Suc-Val-Pro-Phe^P-$(OPh)_2$ gave suitable crystals, which were further examined.

Of this complex, plate-like crystals were grown at 20°C from 1.2 M citrate, pH 7.0, using the hanging drop vapour diffusion technique. These crystals belong to the orthorhombic space group $P2_12_12_1$, have cell constants of a = 40.04 Å, b = 63.61 Å and c = 79.72 Å, diffract X-rays to beyond 1.8 Å resolution, and have one molecule in the asymmetric unit.

The crystals were mounted in 1.3 M citrate, pH 7.0. A complete data set to 1.8 Å was collected on a MAR image plate system (MAR Research, Hamburg, Germany) from a single crystal at 17°C. It was evaluated with the MOSFLM package (Leslie, 1991) and loaded and scaled using ROTAVATA, AGGROVATA and TRUNCATE from the CCP4 program suite (Collaborative Computational Project, 1994). Rotational and translational searches for the determination of the orientation and position of the catg molecules were performed with AMoRe (Navaza, 1994) using data from 12 to 4 Å resolution and bovine β-trypsin (Bode and Schwanger, 1975) as a search model, with all non-identical residues changed to alanine. A unique solution was found with a correlation factor of 39.6 and an *R*-factor of 45.7% (12–4 Å). The corresponding figures of the next best solution were 14.5 and 54.2%.

Crystallographic refinement was done in several cycles consisting of model-building performed with MAIN (Turk, 1992) and conjugate gradient minimization and simulated annealing using X-PLOR (Brünger, 1992). The target parameters of Engh and Huber (1991) were used. This procedure converged rapidly, yielding a good model (see Table II). Individual, restrained atomic B-values were refined, and no sigma cut-off was applied in the whole procedure. The electron density accounting for the inhibitor built in at an R-value of 29.1% at 8–1.8 Å resolution was clearly visible before including it in phasing. The bond between Ser195 Oγ and PhoI4 P was realized as a patch residue in X-PLOR. Very weak angle restraints (~1/10 of normal values) around this covalent inhibitor–protein bond were chosen to allow unbiased angle refinement. An additional simulated annealing protocol with very weak restraints for the Ser195 Oγ-PhoI4 P bond yielded a bond length of 1.61 Å. Some 10% of the reflections were omitted from the refinement before a simulated annealing run of the model to 4000 K, yielding an free *R*-value of 24%. Except for a five-residue segment from Gln36 to Gly38, the whole main chain is in appropriate electron density. Only a few side chains projecting into the solvent are partially or fully undefined in the electron density; the occupancy of all undefined atoms was set to zero.

Accession numbers

The coordinates and structure factors for CATG have been deposited with the Protein Data Bank with the ID codes 1CGH (coordinates) and R1CGHSF (structure factors).

Acknowledgements

We thank Andreas Bergner for assistance in data evaluation, Dr Richard A.Engh for critically reading the manuscript, Dr Dieter Jenne, Dr Jan Löwe and Stefan Steinbacher for helpful discussions, and the SFB 207 (W.B.) for financial support.

References

Allen,D.H. and Tracy,P.B. (1995) Human coagulation factor V is activated to the functional cofactor by elastase and cathepsin G expressed at the monocyte surface. *J. Biol. Chem.*, **270**, 1408–1415.

Avril,L.E., di Martino-Ferrer,M., Pignede,G., Seman,M. and Gauthier,F. (1994) Identification of the U-937 membrane-associated proteinase interacting with the V3 loop of HIV-1 gp120 as cathepsin G. *FEBS Lett.*, **345**, 81–86.

Avril,L.E., di Martino-Ferrer,M., Brillard-Bourdet,M. and Gauthier,F. (1995) Inhibition of U-937 membrane-associated cathepsin G by GP120 (IIIB) and V3 loop-derived peptides from several strains of HIV-1. *FEBS Lett.*, **367**, 251–256.

Baggiolini,M., Schnyder,J., Bretz,U., Dewald,B. and Ruch,W. (1979) Cellular mechanisms of proteinase release from inflammatory cells and the degradation of extracellular proteins. *Ciba Foundation Symposium*, **75**, 105–121.

Bangalore,N. and Travis,J. (1994) Comparison of properties of membrane bound versus soluble forms of human leukocytic elastase and cathepsin G. *Biol. Chem. Hoppe-Seyler*, **375**, 659–666.

Bangalore,N., Travis,J., Onunka,V.C., Pohl,J. and Shafer,W.M. (1990) Identification of the primary antimicrobial domains in human neutrophil cathepsin G. *J. Biol. Chem.*, **265**, 13584–13588.

Barton,G.J. (1993) ALSCRIPT: a tool to format multiple sequence alignments. *Prot. Engng*, **6**, 37–40.

Baugh,R.J. and Travis,J. (1976) Human leukocyte granule elastase: rapid isolation and characterization. *Biochemistry*, **15**, 836–841.

Beatty,K., Bieth,J. and Travis,J. (1980) Kinetics of association of serine proteinases with native and oxidized alpha-1-proteinase inhibitor and alpha-1-antichymotrypsin. *J. Biol. Chem.*, **255**, 3931–3934.

Bertrand,J.A., Oleksyszyn,J. Kam,C.-M., Boduszek,B., Presnell,S., Plaskon,R.R., Suddath,F.L., Powers,J.C. and Williams,L.D. (1996) Inhibition of trypsin and thrombin by amino (4-amidinophenyl) methanephosphonate diphenyl ester derivatives: X-ray structures and molecular models. *Biochemistry*, **35**, 3147–3155.

Blevins,R.A. and Tulinsky,A. (1985) The refinement and the structure of the dimer of α-chymotrypsin at 1.67 Å resolution. *J. Biol. Chem.*, **260**, 4264–4275.

Bode,W. (1996) The three-dimensional structure of human neutrophil elastase. In Crystal,R.G. (ed.), *Lung Biology in Health and Disease.* Marcel Dekker, Inc., New York, Vol. 88, pp. 97–117.

Bode,W. and Huber,R. (1986) Crystal structures of pancreatic serine endopeptidases. In Desnuelle,P. (ed.), *Molecular and Cellular Basis of Digestion.* Elsevier, Amsterdam, pp. 213–234.

Bode,W. and Schwager,P. (1975) The refined crystal structure of bovine β-trypsin at 1.8 Å resolution. II. Crystallographic refinement, calcium binding site, benzamidine binding site and active site at pH 7.0. *J. Mol. Biol.*, **98**, 693–717.

Bode,W., Wei,A.Z., Huber,R., Meyer,E., Travis,J. and Neumann,S. (1986) X-ray crystal structure of the complex of human leukocyte elastase (PMN elastase) and the third domain of the turkey ovomucoid inhibitor. *EMBO J.*, **5**, 2453–2458.

Brandstetter,H., Bauer,M., Huber,R., Lollar,P. and Bode,W. (1995) X-ray structure of clotting factor IXa: active site and module structure related to Xase activity and hemophilia B. *Proc. Natl Acad. Sci. USA*, **92**, 9796–9800.

Brinkmann,T., Schnierer,S. and Tschesche,H. (1991) Recombinant aprotinin homologue with new inhibitory specificity for cathepsin G. *Eur. J. Biochem.*, **202**, 95–99.

Brünger,A. (1992) *X-PLOR Version 3.1, A System for X-ray Crystallography and NMR.* Yale University Press, New Haven, CT.

Campbell,E.J., Silverman,E.K. and Campbell,M.A. (1989) Elastase and cathepsin G of human monocytes. Quantification of cellular content, release in response to stimuli, and heterogeneity in elastase-mediated proteolytic activity. *J. Immunol.*, **143**, 2961–2968.

Caputo,A., James,M.N.G., Powers,J.C., Hudig,D. and Bleakley,R.C. (1994) Conversion of the substrate specificity of mouse proteinase granzyme B. *Nature Struct. Biol.*, **1**, 364–367.

Caughey,G.H. (1994) Serine proteinases of mast cell and leukocyte granules. A league of their own. *Am. J. Respir. Crit. Care Med.*, **150**, S138–S142.

Chandrasekharan,U.M., Sanker,S., Glynias,M.J., Karnik,S.S. and Husain,A. (1996) Angiotensin II-forming activity in a reconstructed ancestral chymase. *Science*, **271**, 502–505.

Collaborative Computational Project (1994) The CCP4 Suite: programs for protein crystallography. *Acta Crystallogr.*, **D50**, 760–763.

Engh,R.A. and Huber,R. (1991) Accurate bond and angle parameters for X-ray protein structure and refinement. *Acta Crystallogr.*, **A47**, 392–400.

Ermolieff,J., Boudier,C., Laine,A., Meyer,B. and Bieth,J.G. (1994) Heparin protects cathepsin G against inhibition by protein proteinase inhibitors. *J. Biol. Chem.*, **269**, 29502–29508.

Faber,J.P., Poller,W., Olek,K., Baumann,U., Carlson,J., Lindmark,B. and Eriksson,S. (1993) The molecular basis of alpha 1-antichymotrypsin deficiency in a heterozygote with liver and lung disease. *J. Hepatol.*, **18**, 313–321.

Fioretti,E., Angeletti,M., Coletta,M., Ascenzi,P., Bolognesi,M., Menegatti,E., Rizzi,M. and Ascoli,F. (1993) Binding of bovine basic pancreatic trypsin inhibitor (Kunitz) as well as bovine and porcine pancreatic secretory trypsin inhibitor (Kazal) to human cathepsin G: a kinetic and thermodynamic study. *J. Enzyme Inhibition*, **7**, 57–64.

Frommherz,K.J., Faller,B. and Bieth,J.G. (1991) Heparin strongly decreases the rate of inhibition of neutrophil elastase by alpha 1-proteinase inhibitor. *J. Biol. Chem.*, **266**, 15356–15362.

Gabay,J.E. (1994) Antimicrobial proteins with homology to serine proteases. *Ciba Foundation Symposium*, **186**, 237–247, 247–249.

Garwicz,D., Lindmark,A. and Gullberg,U. (1995) Human cathepsin G lacking functional glycosylation site is proteolytically processed and targeted for storage in granules after transfection to the rat basophilic/mast cell line RBL or the murine myeloid cell line 32D. *J. Biol. Chem.*, **270**, 28413–28418.

Griffiths,G.M. and Isaaz,S. (1993) Granzymes A and B are targeted to the lytic granules of lymphocytes by the mannose-6-phosphate receptor. *J. Cell Biol.*, **120**, 885–896.

Gullberg,U., Lindmark,A., Nilsson,E., Persson,A.M. and Olsson,I. (1994) Processing of human cathepsin G after transfection to the rat basophilic/mast cell tumor line RBL. *J. Biol. Chem.*, **269**, 25219–25225.

Haddad,P., Jenne,D., Tschopp,J., Clement,M.V., Mathieu-Mahul,D. and Sasportes,M. (1991) Structure and evolutionary origin of the human granzyme H gene. *Int. Immunol.*, **3**, 57–66.

Hartley,B.S. and Shotton,D.M. (1971) Pancreatic elastase. In Boyer,P.D. (ed.), *The Enzymes.* Academic Press, New York, Vol. III, pp. 323–373.

Hase-Yamazaki,T. and Aoki,Y. (1995) Stimulation of human lymphocytes by cathepsin G. *Cell. Immunol.*, **160**, 24–32.

Jenne,D.E., Masson,D., Zimmer,M., Haefliger,J.-A., Li,W.-H. and Tschopp,J. (1989) Isolation and complete structure of the lymphocyte serine protease granzyme G, a novel member of the granzyme multigene family in murine cytolytic T lymphocytes. Evolutionary origin of lymphocyte proteases. *Biochemistry*, **28**, 7953–7961.

Kraulis,P.J. (1991) MOLSCRIPT: a program to produce both detailed and schematic plots of protein structures. *J. Appl. Crystallogr.*, **24**, 946–950.

Leslie,A.G.W. (1991) *Recent Changes to the MOSFLM Package for Processing Film and Image Plate Data.* SERC Laboratory, Daresbury, Warrington WA4 4AD, UK.

Maison,C.M., Villiers,C.L. and Colomb,M.G. (1991) Proteolysis of C3 on U937 cell plasma membranes. Purification of cathepsin G. *J. Immunol.*, **147**, 921–926.

McGuire,M.J., Lipsky,P.E. and Thiele,D.L. (1993) Generation of active myeloid and lymphoid granule serine proteases requires processing by the granule thiol protease dipeptidyl peptidase I. *J. Biol. Chem.*, **268**, 2458–2467.

Merritt,E.A. and Murphy,M.E.P. (1994) Raster3D version 2.0. A program for photorealistic molecular graphics. *Acta Crystallogr.*, **D50**, 869–873.

Mikes,O., Holeysovsky,V., Tomasek,V. and Sorm,F. (1966) Covalent structure of bovine trypsinogen. The position of the remaining amides. *Biochem. Biophys. Res. Commun.*, **24**, 346–352.

Molino,M., Blanchard,N., Belmonte,E., Tarver,A.P., Abrams,C., Hoxie,J.A., Cerletti,C. and Brass,L.F. (1995) Proteolysis of the human platelet and endothelial cell thrombin receptor by neutrophil-derived cathepsin G. *J. Biol. Chem.*, **270**, 11168–11175.

Murphy,M.E.P., Moult,J., Bleackley,R.C., Gershenfeld,H., Weissman,I.L. and James,M.N.G. (1988) Comparative molecular model building of two serine proteinases from cytotoxic T lymphocytes. *Proteins*, **4**, 190–204.

Navaza,J. (1994) Amore – an automated package for molecular replacement. *Acta Crystallogr.*, **A50**, 157–163.

Navia,M.A., McKeever,B.M., Springer,J.P., Lin,T.-Y., Wiliams,H.R., Fluder,E.M., Dorn,C.P. and Hoogsten,K. (1989) Structure of human neutrophil elastase in complex with a peptide chloromethyl ketone inhibitor at 1.84-Å resolution. *Proc. Natl Acad. Sci. USA*, **86**, 7–11.

Nicholls,A., Bharadwaj,R. and Honig,B. (1993) Grasp – graphical representation and analysis of surface properties. *Biophys. J.*, **64**, A166.

Oleksyszyn,J. and Powers,J.C. (1994) Amino acid and peptide phosphonate derivatives as specific inhibitors of serine peptidases. *Methods Enzymol.*, **244**, 442–457.

Owen,C.A. and Campbell,E.J. (1995) Neutrophil proteinases and matrix degradation. The cell biology of pericellular proteolysis. *Cell Biol.*, **6**, 367–376.

Padmanabhan,K., Padmanabhan,K.P., Tulinsky,A., Park,C.H., Bode,W., Huber,R., Blankenship,D.T., Cardin,A.D. and Kisiel,W. (1993) Structure of human des(1-45) factor Xa at 2.2 Å resolution. *J. Mol. Biol.*, **232**, 947–966.

Padrines,M., Wolf,M., Walz,A. and Baggiolini,M. (1994) Interleukin-8 processing by neutrophil elastase, cathepsin G and proteinase-3. *FEBS Lett.*, **352**, 231–235.

Powers,J.C. and Harper,J.W. (1986) Inhibitors of metalloproteases. In Barrett,A.J. and Salvesen,G. (eds), *Research Monographs in Cell and Tissue Physiology.* Elsevier, Amsterdam, Vol. 12, pp. 219–298.

Powers,J.C. *et al.* (1985) Mammalian chymotrypsin-like enzymes. Comparative reactivities of rat mast cell proteases, human and dog skin chymases, and human cathepsin G with peptide 4-nitroanilide substrates and with peptide chloromethyl ketone and sulfonyl fluoride inhibitors. *Biochemistry*, **24**, 2048–2058.

Powers,J.C., Kam,C.-M., Narasimhan,L., Oleksyszyn,J., Hernandez,M.A. and Ueda,T. (1989) Mechanism-based isocoumarin inhibitors for serine proteases: use of active site structure and substrate specificity in inhibitor design. *J. Cell. Biochem.*, **39**, 33–46.

Reilly,C.F., Tewksbury,D.A., Schechter,N.M. and Travis,J. (1982). Rapid conversion of angiotensin I to angiotensin II by neutrophil and mast cell proteinases. *J. Biol. Chem.*, **257**, 8619–8622.

Remington,S.J., Woodbury,R.G., Reynolds,R.A., Matthews,B.W. and Neurath,H. (1988) The structure of rat mast cell protease II at 1.9 Å resolution. *Biochemistry*, **27**, 8097–8105.

Salvesen,G. and Enghild,J.J. (1990) An unusual specificity in the activation of neutrophil serine proteinase zymogens. *Biochemistry*, **29**, 5304–5308.

Salvesen,G., Farley,D., Shuman,J., Przybyla,A., Reilly,C. and Travis,J. (1987) Molecular cloning of human cathepsin G: structural similarity to mast cell and cytotoxic T lymphocyte proteinases. *Biochemistry*, **26**, 2289–2293.

Savage,M.J., Iqbal,M., Loh,T., Trusko,S.P., Scott,R. and Siman,R. (1994) Cathepsin G: localization in human cerebral cortex and generation of amyloidogenic fragments from the beta-amyloid precursor protein. *Neuroscience*, **60**, 607–619.

Schechter,N.M., Wang,Z.M., Blacher,R.W., Lessin,S.R., Lazarus,G.S. and Rubin,H. (1994) Determination of the primary structures of human skin chymase and cathepsin G from cutaneous mast cells of urticaria pigmentosa lesions. *J. Immunol.*, **152**, 4062–4069.

Schiessler,H., Arnhold,M., Ohlsson,K. and Fritz,H. (1976) Inhibitors of acrosin and granulocyte proteinases from human genital tract secretions. *Hoppe-Seylers Z. Physiol. Chem.*, **357**, 1251–1260.

Selak,M.A. (1994) Cathepsin G and thrombin: evidence for two different platelet receptors. *Biochem. J.*, **297**, 269–275.

Shafer,W.M., Pohl,J., Onunka,V.C., Bangalore,N. and Travis,J. (1991) Human lysosomal cathepsin G and granzyme B share a functionally conserved broad spectrum antibacterial peptide. *J. Biol. Chem.*, **266**, 112–116.

Sinha,S., Watorek,W., Karr,S., Giles,J., Bode,W. and Travis,J. (1987) Primary structure of human neutrophil elastase. *Proc. Natl Acad. Sci. USA*, **84**, 2228–2232.

Snyder,R.A., Kaempfer,C.E. and Wintroub,B.U. (1985) Chemistry of a human monocyte-derived cell line (U937): identification of the angiotensin I-converting activity as leukocyte cathepsin G. *Blood*, **65**, 176–182.

Tanaka,T., Minematsu,Y., Reilly,C.F., Travis,J. and Powers,J.C. (1985) Human leukocyte cathepsin G. Subsite mapping with 4-nitroanilides, chemical modification, and effect of possible cofactors. *Biochemistry*, **24**, 2040–2047.

Travis,J. (1988) Structure, function, and control of neutrophil proteinases. *Am. J. Med.*, **84**, 37–42.

Travis,J., Garner,D. and Bowen,J. (1978) Human alpha-1-antichymotrypsin: purification and properties. *Biochemistry*, **17**, 5647–5651.

Turk,D. (1992) *Weitereentwicklung eines Programmes für Molekülgrafik und Elektronendichte-Manipulation und seine Anwendung auf verschiendene Protein-Strukturaufklärungen*. Technische Universität München, München.

Wei,A.Z., Mayr,I. and Bode,W. (1988) The refined 2.3 Å crystal structure of human leukocyte elastase in a complex with a valine chloromethyl ketone inhibitor. *FEBS Lett.*, **234**, 367–373.

Woodbury,R.G., Katunuma,N., Kobayashi,K., Titani,K. and Neurath,H. (1978) Covalent structure of a group-specific protease from rat small intestine. *Biochemistry*, **17**, 811–819.

Received on May 20, 1996; revised on June 28, 1996